Green Chemistry

PAPER

View Article Online
View Journal | View Issue

Cite this: *Green Chem.*, 2025, **27**, 14695

Sustainable direct recycling of Si/Gr scrap electrodes using water-based methods: a green and scalable delamination approach

Stiven López Guzmán, [a,b] Lisa Schlott, [c] Cristina Luengo,[a] Marine Reynaud, [a] Marcus Fehse *[a] and Montse Galceran *[a]

Silicon–graphite (Si/Gr) composites are emerging as alternative anode materials for lithium-ion batteries because they combine higher energy density with improved storage capacity. As its commercial adoption grows, it is fundamental to develop recycling strategies for the currently most available source of this type of material, the manufacturing scrap. In this pioneering work, we report two water-based, delamination methods: ice-stripping and ultrasound delamination, for the direct recycling of Si/Gr scrap electrodes. Ice-stripping achieves a recovery efficiency of 98 ± 1%, while preserving the material's structural and electrochemical properties. The electrodes retain 94% of the initial capacity (503 mAh g^{-1}) after 100 cycles, closely matching the performance of pristine electrodes. In contrast, ultrasound-assisted delamination shows lower recovery yield and capacity performance. A preliminary environmental and economic analysis highlights ice-stripping as the most cost-effective and sustainable recycling option, with a delamination cost of 1.08$ per kg, reducing cost by ~70% compared to ultrasound and other conventional multiwashing methods. The global warming potential is reduced by 50% (1.2 kg CO_2e per kg) compared to the other delamination techniques, and is more than 30-fold lower than that associated with producing an electrode from pristine Si/Gr. These findings establish a low-impact, scalable pathway for Si/Gr recycling, supporting the development of circular battery manufacturing under upcoming regulatory and sustainability frameworks.

Received 25th August 2025,
Accepted 20th October 2025

DOI: 10.1039/d5gc04489h

rsc.li/greenchem

Green foundation

1. This work establishes a rapid and low-impact route for the direct recycling of Si/Gr scrap, avoiding energy-intensive calcinations or chemical leaching. Using only minimal water and mechanical stimuli, it advances the principles of waste management, safer solvents, and energy efficiency, while enabling electrode reuse directly into production loops.
2. We achieve delamination and recovery of Si/Gr electrodes with negligible solvent use and modest electricity input. Life-cycle calculations show that ice-stripping lowers global warming potential by ~50% compared to other delamination methods (1.2 kg CO_2e per kg) and is >30-fold lower than making pristine electrodes (34.9 kg CO_2e per kg), demonstrating clear environmental and economic benefits.
3. Future work will scale the process under continuous low-energy operation, valorize the Cu current collector, and address Si redistribution in the carbon network further to enhance the circularity and green metrics of the process.

1. Introduction

Climate change has intensified the urgency to reduce CO_2 emissions and mitigate global warming.[1] The rapid deployment of electrochemical energy-storage systems offers a viable pathway to decrease dependence on fossil fuels across key sectors such as mobility and energy generation.[2] Since their commercialization in 1991, lithium-ion batteries (LIBs) have become central to this transition; however, further advancements in energy density, power capability, and cycle life remain essential.

Graphite (Gr) remains the industry-standard anode material due to its low cost, high electrical conductivity, and excellent reversibility. Yet, it can accommodate only one Li per six C atoms, limiting its theoretical gravimetric capacity to 372 mAh g^{-1}.[3] In contrast, silicon (Si) provides a much higher theoretical capacity of 3579 mAh g^{-1} through lithium alloying

[a]*Center for Cooperative Research on Alternative Energies (CIC energiGUNE), Basque Research and Technology Alliance (BRTA), Alava Technology Park, Albert Einstein 48, 01510 Vitoria-Gasteiz, Spain. E-mail: mfehse@cicenergigune.com, mgalceran@cicenergigune.com*
[b]*Chemical and Environmental Engineering Department, Faculty of Science and Technology, University of the Basque Country, UPV/EHU, Bo Sarriena s/n, 48940 Leioa, Spain*
[c]*Institute of Business Administration at the Department of Chemistry and Pharmacy, University of Münster, Leonardo-Campus 1, 48149 Münster, Germany*

to form $Li_{15}Si_4$, offering nearly ten times the capacity of graphite while maintaining comparable cost and abundance.[4] However, Si undergoes a volumetric expansion of approximately 300% during (de)lithiation, which induces particle cracking and continuous solid-electrolyte interphase (SEI) reformation, leading to rapid capacity fade.[5] To mitigate these issues, Si is commonly blended with Gr to buffer mechanical strain and leverage graphite's electronic conductivity, yielding improved cycle stability within the classic "capacity–stability" trade-off relationship.[6,7]

As LIB production scales, large volumes of electrode scrap are generated during the manufacturing process. Discarding these scraps represents a waste of resources and an environmental burden, underscoring the importance of developing efficient recycling strategies.[8] Direct recycling, which focuses on recovering and reusing active materials without the need for extensive reprocessing,[9,10] offers a promising approach for preserving the value of recycled materials, by allowing the direct reintegration into the manufacturing line, thereby reducing costs and minimizing the environmental footprint of the production process.[11,12]

Although direct recycling has demonstrated encouraging results for cathode chemistries such as NMC, LFP, LMO, LNMO, and NCA,[13–17] as well as for anode materials,[18–22] several challenges remain before large-scale commercialization can be achieved. At the industrial level, direct recycling remains limited by strong electrode–collector adhesion, variations in feedstock composition, safety and contamination risks, the lack of infrastructure suited for gentle delamination, and the absence of standardized regulations and material quality metrics.[23–25] Currently, the primary driver for recycling continues to be the economic value of the recovered material, resulting in a focus on cathode recycling due to their higher critical metal content and market value.[26,27] In contrast, anode materials are often overlooked in recycling research despite their growing use and compositional complexity, largely due to the lack of economic motivation for their recycling.[28,29] However, geopolitical concerns and fluctuations in prices have recently drawn attention to the recovery of values for this type of material.

Besides the recycling of graphite having been previously demonstrated and studied, the case of Si/Gr composites remains largely unexplored. The recycling of Si/Gr electrodes presents distinct challenges arising from their heterogeneous microstructure and complex interfacial behavior, which necessitate careful consideration of each component and may require process adjustments depending on the state of the material to be recycled. For spent electrodes, the properties of the Si particles can be altered by the volumetric expansion and SEI formation during lithiation, leading to internal stress, particle fracture, and binder redistribution.[6] In contrast, graphite may exhibit pore clogging and impurities that hinder its electrochemical performance.[30,31] In scrap electrodes, which are the subject of this study, both Si and Gr remain structurally unaltered; the main challenge lies in delaminating the coatings while preserving the composite matrix and crystal structure. As a result, solvent- or heat-based recycling strategies are considered unsuitable for recovering Si/Gr materials, as they may damage the fragile carbon–silicon network and consume large amounts of energy and chemicals.

Previous studies have focused on regenerating spent graphite and subsequently combining it with silicon particles to produce Si/Gr composites.[32,33] However, to our knowledge, no previous study has addressed the direct recycling of Si/Gr composite electrodes sourced from manufacturing scrap. This gap represents a critical barrier in achieving a circular battery economy, particularly as the industrial use of Si/Gr electrodes expands. The necessity of recycling overlooked materials, such as Gr or the novel Si/Gr, aligns with recent European Union regulations mandating a minimum recycled content in batteries,[34] thereby creating both a policy incentive and an industrial need to develop greener and scalable recovery strategies.

To overcome these limitations, this work demonstrates, for the first time, that water-based delamination methods, namely ice-stripping and ultrasound delamination, can effectively separate and recover Si/Gr composite scrap anodes, achieving high recovery yields while preserving the electrochemical performance of the material without altering its structure. Both approaches adhere to the principles of green chemistry, as they eliminate the use of harsh reagents, require minimal energy input, and preserve the integrity of both active materials and current collectors, which can subsequently be reclaimed and reused. Ice-stripping involves wetting the electrode surface, freezing it against a cold substrate, and then mechanically removing the active material from the current collector.[35] This concept has already demonstrated its effectiveness for various negative electrodes, highlighting the robustness of this delamination technique.[19] Ultrasound delamination, by contrast, employs high-frequency acoustic waves to detach active materials from current collectors, thereby enhancing recovery efficiency without inducing chemical degradation.[17,36,37]

Beyond the recovery of materials and the preservation of electrochemical performance, we also present a preliminary gate-to-gate assessment of the delamination and remanufacturing steps, comparing them with a literature-reported multi-washing approach. The analysis quantifies energy and water consumption, direct operating costs, and the associated global warming potential within a European context. Overall, this study represents a first step toward integrating green anode recycling of next-generation Si/Gr materials into industrial-scale lithium-ion battery manufacturing.

2. Experimental section

2.1 Delamination

A novel delamination technique, developed by Chen *et al.* and known as "ice-stripping", was used to remove the Si/Gr coating from the electrodes.[35] The ice-stripping process was conducted with a commercial stainless steel fried ice cream roll machine,

measuring 28 cm by 24 cm, capable of reaching temperatures as low as −20 °C. To induce delamination, the electrode was sprayed with 5 mL of distilled water using a standard spray and then cooled on a surface at approximately −5 °C to −10 °C for 10 seconds. This freezes the water within the electrode's pores, causing complete delamination of the cast materials and detachment of the current collector. The resulting powder (named I–Si/Gr) was collected and dried overnight in a vacuum oven at 80 °C, and the copper collector was reclaimed.

For the ultrasound delamination, the Si/Gr electrodes were cut and immersed in a beaker with 100 mL of distilled water, followed by ultrasound treatment using a Branson Sonifier 250 with a 1/8-inch tapered microtip. This device is capable of delivering a maximum output of 250 W at a frequency of 20 kHz. A continuous wave was applied for eight minutes at 20% of the system's total energy to facilitate delamination. The physical force of the ultrasonic machine facilitates the separation, helped by the dispersion affinity of CMC and SBR in water, resulting in the delamination of the electrode.[17] The resulting solution was filtered with a vacuum pump, and the powder (labeled U–Si/Gr) was recovered and dried under vacuum at 80 °C overnight. A schematic representation of both ice-stripping and ultrasound delamination processes is depicted in the Fig. 1.

2.2 Material characterization

The pristine and recycled Si/Gr materials were characterized by X-ray diffraction (XRD) with a Bruker D8 Discover (LYNXEYE XE detector with the Cu Kα radiation [λ = 1.54060 Å] in the 2θ range 10–80). Le Bail refinements of the XRD patterns were carried out using the FullProf Suite software[38] to determine the unit cell parameters of the graphite and Si phase for each sample.

Raman spectroscopy was performed with a Renishaw spectrometer (Nanonics Multiview 2000) with a wavelength of 532 nm using 1% of laser power with 15 s of exposure time, in two spots, for graphite and silicon particle spots, in triplicate for each sample. The morphological and type of material distribution of the samples were examined by Scanning electron microscope (SEM – FEI Quanta 200 FEG with 10–15 kV with ETD and BESD detectors). The images were processed using ImageJ to provide a rough estimation of the ratio of silicon to graphite in the sample. This was achieved by applying an enhancement filter and using an automatic threshold with noise reduction to count and estimate the area of the bright silicon particles. The FTIR scans were taken in a PerkinElmer Spectrum 400 with a diamond window, with a resolution of 2 and 64 scans. The particle size analysis (PSA) was performed with a Malvern Mastersizer 3000 in air dispersion.

A STA449 F3 Jupiter (Netzsch) was used to evaluate the thermal stability and presence of residuals of the material. The simultaneous thermal analysis (STA) experiments were performed from 30 °C–1000 °C at a heating rate of 10 °C min^{-1} under an argon and synthetic air (80% nitrogen + 20% oxygen) atmosphere with a flow rate of 60 mL min^{-1}. The STA instrument was coupled to a quadrupole mass spectrometer (QMS 403 Aëolos, Netzsch) to analyze the gas mass evolution. Differential thermal analysis (DTA) measures the difference in temperature between the sample and the reference powder, indicating how and whether the sample changes in temperature.

2.3 Cell preparation

Single-sided coated negative electrodes containing 94 wt% mixture of graphite and Si/C (9 wt%), as active material, 2 wt% of C65, and 2 wt% of carboxymethyl cellulose (CMC) TextureCel 2000 and 2 wt% of Styrene–Butadiene Rubber (SBR) TRD 302A were provided by SAFT. The electrodes prepared from the recycled samples were made by adding 2% of binders (1 wt% CMC and 1 wt% SBR) and distilled water to achieve a desired loading of approximately 40 wt% The reclaimed powders were homogenized in a mortar, then mixed with the CMC, SBR, and water solutions, and dispersed with an IKA stirrer until a homogeneous slurry was obtained.

The electrochemical performance of the different samples was analyzed in a climatic chamber with controlled temperature (25 °C) using a CR2032 coin-type cell assembled in a glove box under an Ar atmosphere against metallic lithium. The electrolyte used was $LiPF_6$ in ethyl methyl carbonate : fluoroethylene carbonate (EMC : FEC; 7 : 3) + 2% of vinylene carbonate (VC). All materials were tested in triplicate, and the detailed cycling protocol for electrochemical testing is provided in SI Table S1.

2.4 Economic analysis

A preliminary economic analysis was conducted to examine the benefits and advantages of the water-based delamination techniques. For comparison with the two delamination approaches developed in this work (ice-stripping and ultrasound delamination), the widely used water immersion washing ("multiwashing") method for anode delamination was adopted from the literature.[20,22,39] In this case, the process involves immersing the anode sheets in hot water and washing them several times to remove the binder and conductive carbon.

The three water-based delamination techniques were evaluated in terms of gate-to-gate recovery cost, water consumption, and global warming potential (GWP). The functional unit was defined as 1 kg of recovered active anode material. The system boundary covered the delamination step and the re-manufacturing of a new electrode coating using the recovered material. Cost estimates were derived from laboratory-scale process data, including consumables (such as water and electricity), process time, and additive replenishment (*e.g.*, binder). Energy consumption was calculated by scaling the operational power demand of the respective equipment (*e.g.*, ultrasonic bath, ice stripping apparatus) to the per-kilogram throughput. Water use was measured directly during experiments and scaled according to process volumes. The drying step was assumed identical across all processes, with no scaling applied, as the laboratory oven accommodates a batch size equivalent to 1 kg of active material.

The GWP was calculated using the IPCC 2021 GWP100 method, applying economic allocation, with life cycle inven-

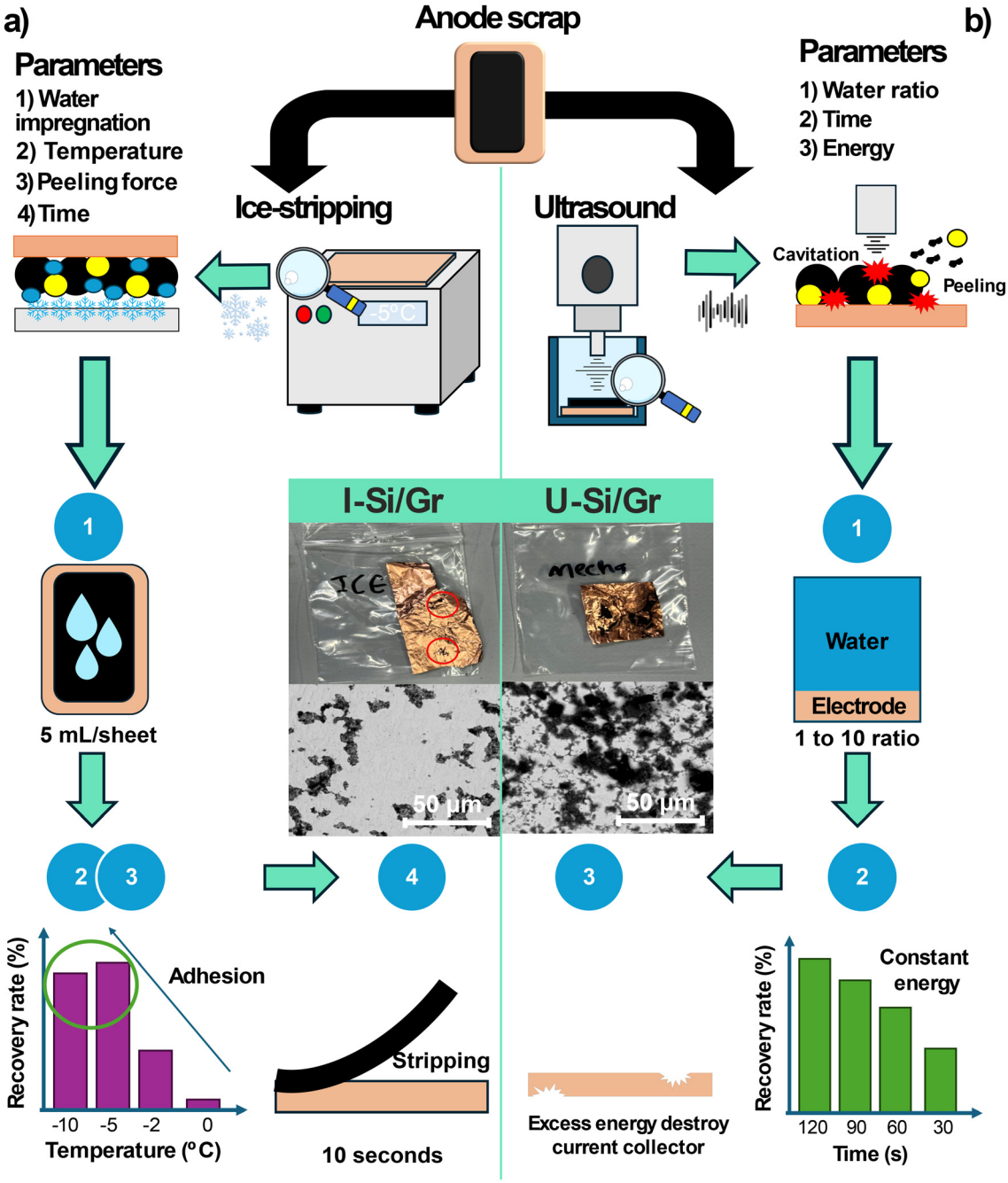

Fig. 1 Schematic of the two delamination routes applied to Si/Gr anode scrap. (a) Ice-stripping: water impregnation, temperature, peeling force, and time govern the delamination efficiency; with higher recovery at lower temperatures, which also increases the adhesion. (b) Ultrasound delamination: water ratio, duration, and energy determine recovery; a 1 : 10 electrode-to-water ratio gave optimal detachment, while excess energy damaged Cu. Center SEM images show recovered electrodes (I–Si/Gr, U–Si/Gr) and corresponding Cu surfaces, confirming effective, water-based delamination.

tory (LCI) data sourced from Ecoinvent 3.11. Standard emission factors for electricity, water, and pristine graphite production were applied. Pristine anode material production (94 wt% SiGr, 2 wt% C65, 2 wt% CMC, 2 wt% SBR) was included as a benchmark scenario. All assumptions, inventory data, and calculation procedures are detailed in the SI.

3. Results

3.1 Electrode delamination

Si/Gr scrap electrodes were tested under two delamination processes (Fig. 1), an ice stripping delamination,[35] and an ultrasound delamination, which allows the green and direct recovery of the anode active materials and current collectors.

The working mechanism of the ice-stripping consists of an interplay between water penetration, temperature, adhesion strength, and contact time of the coating, which determines the efficiency of the ice-stripping process, see Fig. 1a.

During delamination, a thin layer of water (5 mL per sheet) infiltrates the porous Si/Gr coating and reaches the interface with the current collector. Upon placing the wetted electrode on a cold plate maintained at a temperature between −5 °C and −10 °C, the water film rapidly freezes, resulting in volumetric expansion. This transition creates both normal and shear stresses at the coating–collector interface, which exceed the weaker adhesion forces between the coating and current collector. When these stresses exceed the interfacial adhesion, cracks initiate and propagate, allowing the layer to detach cleanly while leaving the collector residue-free.

Temperature plays a key role in this process: according to Chen *et al.*,[35] the onset of effective delamination occurs below −4 °C, and full recovery is achieved near −10 °C. Contact time is equally critical, as the freezing of the interfacial water film must be sufficient to establish a cohesive "ice-tape" between the coating and the cold substrate. This time can be estimated from Newton's law of cooling, which models the heat transfer between the electrode and the cold plate:

$$T_c = \frac{mc(T_i - T_f)}{hA} \quad (1)$$

where T_c is the cooling time (s), m the mass of water (kg), c the specific heat of water (4200 J kg^{-1} °C^{-1}),[35] T_i and T_f the initial and final temperatures (25 and 0 °C, respectively), h the heat transfer coefficient (6000–7500 W m^{-2} °C^{-1}),[40] and A the contact area (m^2). For a coating of 9.6 × 6 cm^2, the freezing time ranges between 2.8–3.5 s, confirming that heat transfer and freezing occur faster than heat can diffuse through the surrounding medium.[41]

The rapid solidification of ice allows it to bond effectively to the cold plate, creating interfacial stress on the coating. The lower the temperature and the longer the contact time, the greater the adhesion. Factors such as water penetration and wettability also impact the efficiency of delamination. Higher porosity and hydrophilic binder systems enable deeper water infiltration, promoting more uniform ice formation at the interface.[42] Combining proper wetting, sub-zero temperatures, and adequate freezing time creates interfacial stresses that surpass the adhesion strength of the material. This enables effective delamination while preserving the integrity of the recovered coating.

In the case of the ultrasound delamination, the working principle relies on the application of high-energy ultrasonic waves in a solvent medium. The key factors in this case are the water ratio, sonication duration, and energy used, see Fig. 1b.

To allow the effective delamination, from our previous work, we found that a ratio of 1/10 sample/solvent with 8 minutes of sonication time and 20% of the system total energy allows the effective delamination of most of the material.[17] The ultrasonic waves generate cavitation that is absorbed on the surface of the electrodes. This process creates an aggregation of anode particles, which leads to the breaking of the bonds between the cast material and the current collector, allowing for progressive delamination of the electrode.

As a result, the coating is delaminated and dispersed in the water solution, allowing the metallic current collector to be recovered almost completely clean, with some remains of materials still present on the surface, see Fig. 1b. When attempting to increase the energy or duration of sonication, the current collector began to deteriorate, resulting in pieces of copper being mixed with the delaminated powder, which marks a limitation of this method, at least with our current setup.

Fig. 1 provides an inset image of the recovered current collectors and the corresponding SEM micrograph. Both delamination methods effectively removed most of the active material, and no significant damage or morphological degradation was observed on the surface of the current collector after the delamination process, compared to the pristine Cu (SI Fig. S1), suggesting its suitability for direct reuse.[43] However, some isolated regions with incomplete removal exhibit residual traces of active material and binder/conductive additives, which are more evident in the ultrasound-delaminated samples. Still, the remaining material can be easily cleaned, and it is possible to recover the metallic current collectors completely with no contamination or damage.

3.2 Material flow balance and circularity indicators

As a first step after the delamination of the pristine electrodes (P–Si/Gr), the recovery efficiency was determined by comparing the initial mass to the weight of the recovered powders and current collectors. To make the link to circularity explicit, we quantified the mass flows during delamination (Fig. 2). The coating recovery efficiency (η_{sec}) is defined as:

$$\eta_{rec}\,[\%] = \frac{m_{recovered}}{m_{initial}} \times 100, \quad (2)$$

where $m_{initial}$ is the initial coating mass on the scrap electrode and $m_{recovered}$ is the mass of detached Si/Gr coating. Ice stripping achieved 98 ± 1% recovery efficiency, while ultrasound delivered 88 ± 2%. In both cases, the Cu foil was reclaimed intact (~100%). The resulting powders are a mixture of active material and a certain percentage of additives, which was determined by thermogravimetry and FTIR, and later discussed in the document.

To quantify circularity under direct recycling conditions, we define the Material Retention Ratio (MRR) as:

$$\mathrm{MRR}\,[\%] = \frac{m_{reused}}{m_{input}} \times 100, \quad (3)$$

where m_{input} is the mass of the initial electrode coating and m_{reused} the mass recovered in a form suitable for direct re-manufacturing. For the Si/Gr system. Considering that we estimated the amount of retained active material, binder, and carbon by thermal analysis and microscopy, we were able to determine the amount of material that needs to be readjusted for re-manufacturing. Ice-stripping achieved a recovery of

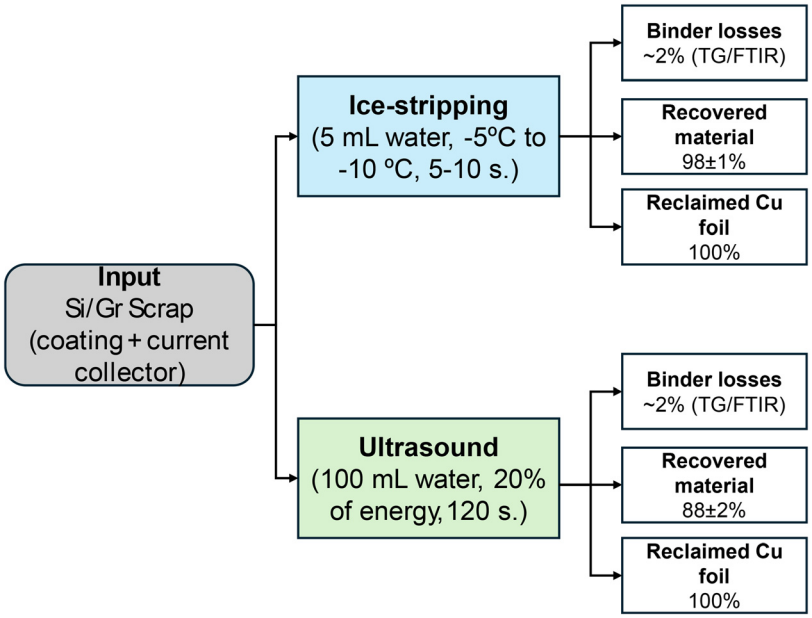

Fig. 2 Material flow balance for water-based delamination routes. The diagram illustrates the distribution of mass between recovered coating, reclaimed Cu foil, and minor binder or fine losses, which serve as preliminary circularity indicators.

m_{input} = 6.6 g from an input of m_{input} = 6.8 g, corresponding to an MRR of 95.1%. Ultrasound delamination yielded 6.0 g, giving an MRR of 86.5% (see Table 1). Reflecting minimal losses in the physical separation step and alignment with circular manufacturing principles based on direct reuse.[44]

3.3 Structural characterization

To investigate the structural preservation of the recovered materials, X-ray diffraction (XRD) and Raman spectroscopy were employed. Fig. 3a shows that all samples exhibit a strong graphite (002) reflection at ~26.5°, characteristic of a high graphitization degree.[45] Additional diffraction peaks corresponding to the Si (111), (220), (311), and (331) planes are also observed, confirming the presence of crystalline silicon.[46] The extracted crystallographic parameters—including the interlayer spacing (d_{002}), crystallite dimensions (L_a, L_c), graphitization degree, and relative peak intensities—are summarized in Table 2, with detailed calculation procedures provided in the SI.

Le Bail fitting of the XRD data (SI Fig. S2) confirms that the graphite lattice parameters remain unchanged after recycling, showing values similar to those of the pristine (P–Si/Gr) sample and consistent with literature reports (see Table 2).[47] These results indicate that the core crystalline framework of graphite remains structurally stable and unaffected by the delamination processes. The interlayer spacing d_{002} (~0.336 nm) is consistent across all samples, in excellent agreement with reported values for graphitic materials.[48] However, minor variations are observed in the degree of graphitization. The P–Si/Gr sample exhibits a high graphitization degree (99%), characterized by large in-plane crystallite sizes (L_a ~73 nm) and a well-preserved stacking height (L_c ~41 nm).[49] Both I–Si/Gr and U–Si/Gr samples display comparable in-plane crystallite sizes (L_a ~77–76 nm, respectively), indicating similar graphitic domain dimensions. Nevertheless, a modest reduction in stacking height is noted, particularly for the ultrasound-treated sample (L_c ~38 nm) compared with the ice-stripped one (L_c ~42 nm), suggesting that the layered structure is better preserved during ice-stripping. Correspondingly, the graphitization degree decreases slightly to 91% for I–Si/Gr and 90% for U–Si/Gr, yet both remain within the range of highly graphitic materials.[50] Regarding the silicon phase, both pristine and recycled samples maintain similar Si lattice parameters ($a \approx 5.431$ Å).

Raman spectroscopy was performed at multiple spots to account for spatial confinement and sample inhomogeneity—specifically on the surface of graphite and silicon particles. The Raman spectrum of the P–Si/Gr particle exhibits a lower I_d/I_g ratio (0.241), indicating a higher degree of structural order. In contrast, both recycled graphite particles display increased disorder, with I_d/I_g ratios of ~0.54 (I–Si/Gr) and 0.58 (U–Si/Gr), suggesting greater structural defects and the presence of residual binder or conductive carbon on the particle surface.[31] The Raman spectrum of the Si region (SI Fig. S3) exhibits a characteristic Si peak at 517 cm^{-1} and similar I_d/I_g ratios (0.65), along with features attributed to disordered carbon, likely originating from the synthesis process.[51]

Table 1 Summary of recovery and circularity metrics for water-based delamination

Process	η_{rec} [%]	Cu foil recovery [%]	MRR [%]
Ice stripping	98 ± 1	~100	95–98
Ultrasound	92 ± 2	~100	89–93

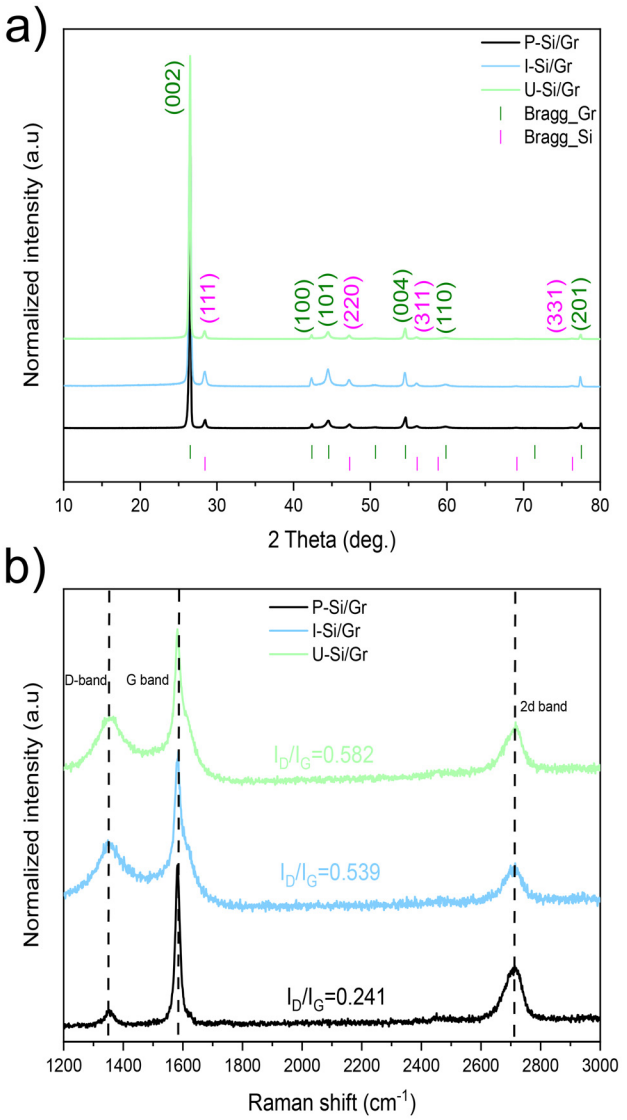

Fig. 3 (a) XRD patterns and (b) Raman spectra of the different Si/Gr samples. Bragg reflections correspond to graphite (ICSD-230104) and Si (ICSD-51688), as referenced from database.

3.4 Morphology analysis of recycled powders

SEM images reveal two key morphological trends (Fig. 4). In the P–Si/Gr sample, the round Si particles (appearing as bright violet features) are homogeneously distributed within a matrix of plate-like graphite flakes. In contrast, the U–Si/Gr sample shows more compact and flattened graphite domains, accompanied by a visibly reduced number of Si particles, suggesting possible Si loss or redistribution during ultrasound delamination. By comparison, the I–Si/Gr samples retain a morphology that closely resembles the pristine sample, with well-dispersed Si particles and an intact graphite network.

Energy-dispersive X-ray spectroscopy (EDX) coupled with SEM (SI Fig. S4) confirms that the Si-to-Gr content in the recovered materials remains close to 9 at%, with only minor variations in the atomic ratio among samples. Given the semi-quantitative nature of EDX, these results are considered orientative. Despite the morphological differences, the overall Si-to-graphite areal ratio and spatial distribution remain consistent across all samples. A close-up SEM image (SI Fig. S5) reveals the characteristic oval morphology of Si particles and the flake-like structure of the graphite. Fragmented Si particles can be observed in the U–Si/Gr samples, along with surface stains on the graphite flakes, which are likely side effects of the ultrasound delamination process.[52]

3.5 Determination of the residual binder content

To evaluate the retention of binder and conductive carbon, thermogravimetric analysis (TG) was performed in both synthetic air and argon atmospheres on reference additives, pristine electrodes, and recycled Si/Gr powders. Differential thermogravimetric (DTG) and differential thermal analysis (DTA) signals were also acquired to identify decomposition events (Fig. 5). Fig. 5a shows the TG/DTG profiles of the individual components SBR, CMC, and C65. CMC displays three distinct degradation stages, featuring a main DTG peak at 275 °C and a shoulder at approximately 400 °C, corresponding to carbonate decomposition.[53] SBR decomposes between 325–475 °C with a primary peak centered at 425 °C,[54] whereas C65 remains stable up to 600 °C and undergoes complete oxidation near 980 °C.

The TG profiles of the pristine and recycled powders in air (Fig. 5b) display distinct multistep mass losses. The DTG curves reveal three main decomposition stages: (1) 220–300 °C (CMC), (2) 300–400 °C (SBR), and (3) above 500 °C, corresponding to the combustion of carbonaceous components. DTA analysis (Fig. 5c) confirms these transitions, showing overlapping exothermic and endothermic peaks. A broad exothermic signal attributed to Si oxidation is most pronounced in the pristine and I–Si/Gr samples but notably attenuated in U–Si/Gr, suggesting partial Si loss caused by cavitation during ultrasonic

Table 2 Crystal and structural parameters of the different samples

	Unit cell parameters Gr		Unit cell parameters Si					
Sample	a (Å)	c (Å)	$a = b = c$ (Å)	d_{002} (nm)	L_a (nm)	L_b (nm)	Graphitization (%)	I_d/I_g
P–Si/Gr	2.461(1)	6.719(1)	5.432(1)	0.3357	73	41	99	0.241
I–Si/Gr	2.461(1)	6.718(4)	5.431(2)	0.3361	77	42	91	0.539
U–Si/Gr	2.462(1)	6.725(4)	5.436(4)	0.3362	76	38	90	0.582

L_a and L_b correspond to in-plane and stacking crystallite sizes, respectively. Graphitization degree was estimated from the d_{002} spacing. The formulas to calculate all these values are reported in the SI.

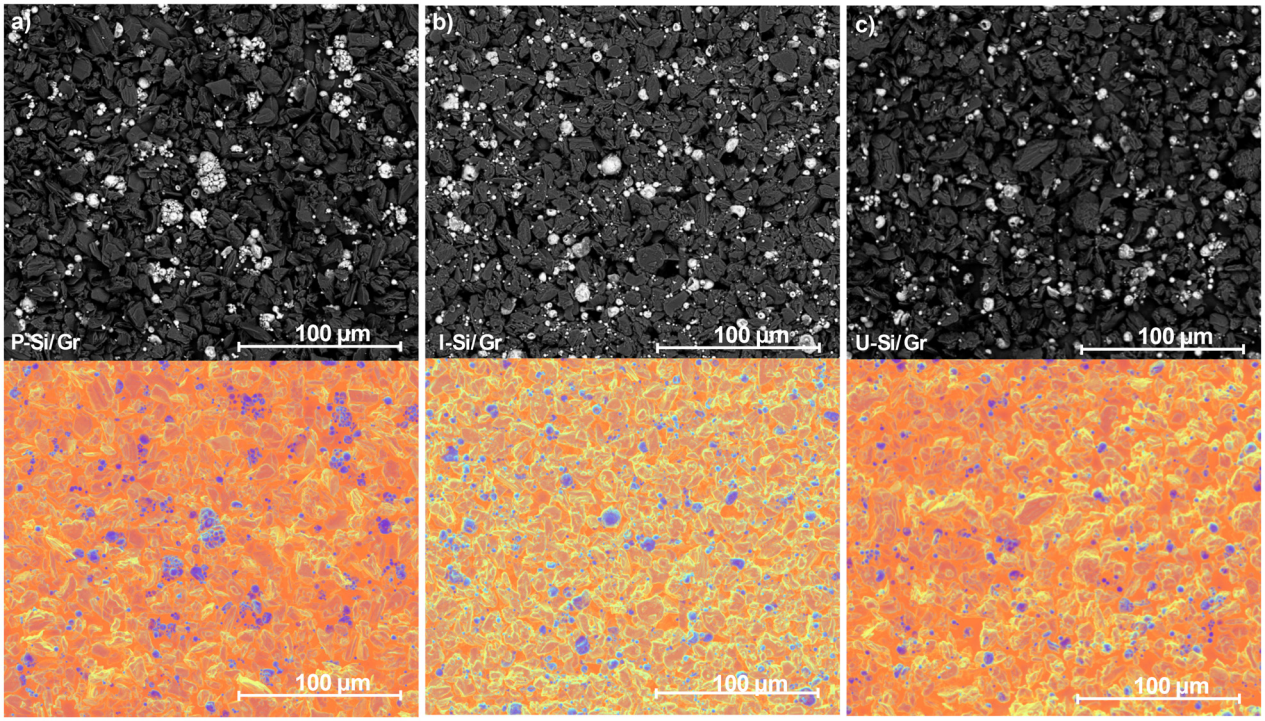

Fig. 4 Top-view SEM micrographs of the Si/Gr anode powders: (a) pristine (P–Si/Gr), (b) ice-delaminated (I–Si/Gr), and (c) ultrasound-delaminated (U–Si/Gr). The top panels correspond to backscattered electron (BSD) images highlighting elemental contrast and particle distribution across the surface. The bottom panels present combined EDS/ETD overlays illustrating the topographical distribution and exposure of Si- and C-rich regions on the recovered powder surface.

delamination.[55] A distinct Cu → CuO oxidation peak at approximately 815 °C appears only in the pristine electrode, confirming the absence of Cu contamination in the recycled materials.

Mass spectrometry (Fig. 5d–f) identifies the evolved gases during oxidation. The recycled powders exhibit a sequential emission of H_2O, CO_2, and O_2, corresponding to the degradation of polymeric and carbonaceous species. The mass loss proceeds through three well-defined steps: (1) H_2O release below 300 °C, associated with moisture removal and CMC decomposition; (2) subsequent release of CO_2 and O_2 linked to binder degradation; and (3) final emission of CO, CO_2, and O_2 from carbon combustion. Based on the ~2.29% binder mass loss detected under argon, it is estimated that approximately 2% polymer content remains in the recycled powders.

Complementary thermogravimetric-mass spectrometry (TG–MS) measurements under an inert (argon) atmosphere are provided in the SI (Fig. S6). These analyses confirm a residual binder content of approximately 2.29 wt%, attributed to the volatilization of SBR and CMC without significant carbon loss or Si oxidation. FTIR spectroscopy (SI Fig. S7) further corroborates the presence of residual binder, showing characteristic absorption bands corresponding to the carboxyl and alkyl groups of CMC and SBR in both I–Si/Gr and U–Si/Gr powders. Moreover, particle size distribution analysis (SI Fig. S8) reveals an approximately 20% increase in Dv50 for the recycled samples, consistent with the agglomeration of particles caused by residual binder.

To restore the original 4 wt% binder formulation, a 2 wt% binder top-up was added during electrode remanufacturing.[56] It is important to consider the residual binder and conductive carbon present in the recovered powders, as assuming a completely pure material or an inaccurate percentage can directly influence the measured electrochemical performance by misrepresenting the accurate active material content in the electrode.[17] Our previous work demonstrated that the retention and reuse of residual binder and conductive carbon are feasible[57] and do not adversely affect the electrochemical performance of the recycled electrodes. However, additional mixing time is required to achieve homogeneous dispersion and ensure consistency in both the slurry and the resulting electrode coating.

3.6 Electrochemical performance

The voltage profiles (Fig. 6a) reveal nearly identical electrochemical behavior for the P–Si/Gr and I–Si/Gr electrodes, exhibiting the typical graphite plateau (≈0.12–0.20 V *vs.* Li/Li^+) and the characteristic sloping region of silicon below 0.1 V. This confirms the preservation of both electrochemically active graphite and silicon domains. A more detailed analysis of these contributions is provided by the differential capacity curves (dQ/dV) (SI Fig. S9).[58] Together with the preceding structural and compositional results, these findings demonstrate that ice-stripping is the most effective approach for preserving electrochemical performance in recycled Si/Gr electrodes.

The cycling performance of the recycled electrodes over 100 cycles is shown in Fig. 6b. The I–Si/Gr sample retains 94% of

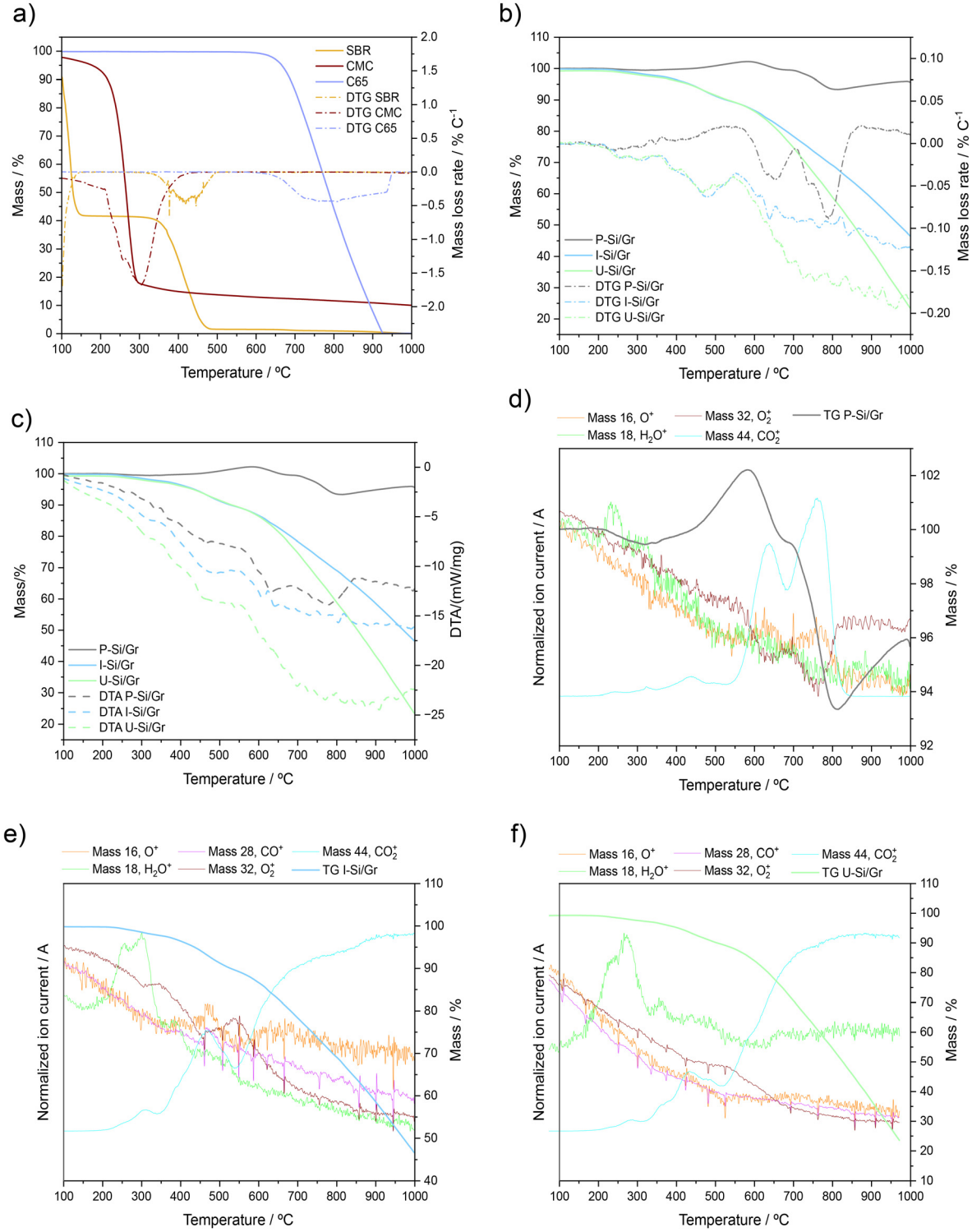

Fig. 5 (a) Reference TG (solid) and DTG (dotted) curves for SBR, CMC, and C65 recorded in air and normalized to unit area. (b) TG (solid) and DTG (dashed) curves of P–Si/Gr (black), I–Si/Gr (blue), and U–Si/Gr (green) in air. (c) Corresponding DTA traces (dashed; exotherm down) overlapped on the TG curves. (d–f) Mass spectroscopy in air reveals distinct mass releases for P–Si/Gr, I–Si/Gr, and U–Si/Gr, respectively.

its initial charge capacity (503 mAh g^{-1}), closely matching the P–Si/Gr electrode, which retains 97% (536 mAh g^{-1}) of the practical capacity (550 mAh g^{-1}) for this Si/Gr composition. In contrast, the U–Si/Gr electrode exhibits the lowest initial capacity (443 mAh g^{-1}) and a more pronounced capacity fade during cycling. All electrodes show an initial coulombic efficiency (ICE) of approximately 90%, higher than typical values reported for similar Si/Gr systems, likely due to the opti-

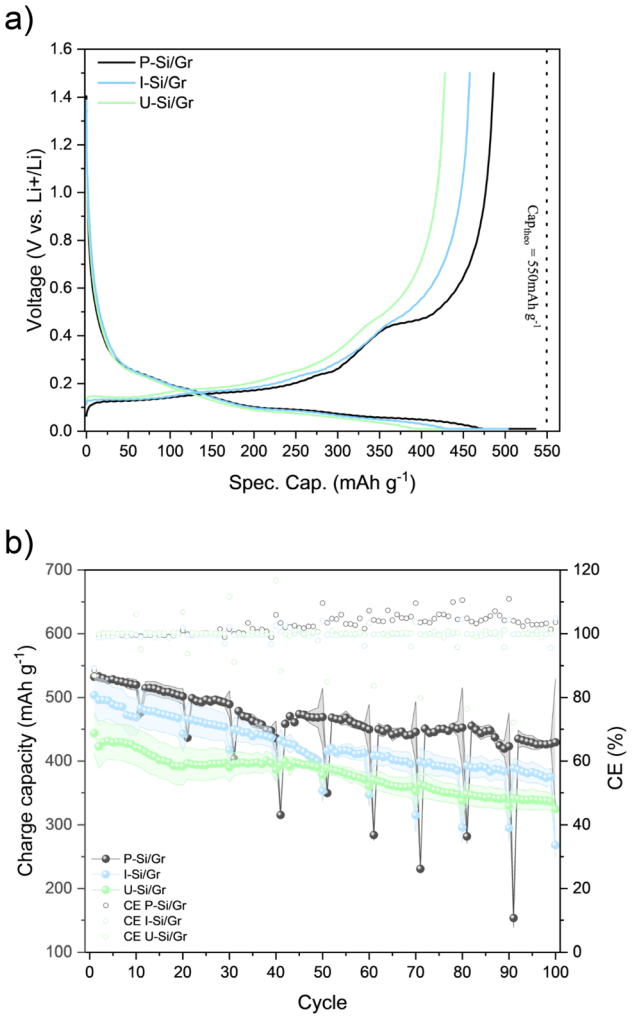

Fig. 6 (a) Voltage profile of the third cycle at C/10. (b) Cycling performance (solid lines, left axis) and coulombic efficiency (CE, hollow circle, right axis) of pristine (P–Si/Gr), and recycled (I–Si/Gr and U–Si/Gr) half-cells over 100 cycles at different C-rates.

mized electrode formulation and structural integrity of the recycled material.[59] The initial ICE is primarily limited by the formation of the SEI, particularly on the silicon surfaces during the first lithiation.[60] The comparable coulombic efficiencies across all samples suggest that the green delamination routes employed here do not introduce surface contamination or alter the intrinsic reactivity of the recovered materials.

The variability across three independent cells per sample is presented by the shaded region in Fig. 6b. Both I–Si/Gr and P–Si/Gr exhibit narrow spread and high reproducibility, while U–Si/Gr displays larger deviations, likely due to inhomogeneous active material distribution and compromised electrode integrity after ultrasonic treatment.

The periodic drops observed in the capacity curves correspond to cycles tested at 3 C. Under these conditions, kinetic limitations such as lithium-ion diffusion within the Si domains and staging transitions in graphite become rate-limiting, while increased polarization accelerates cutoff potentials and reduces the accessible capacity. In addition, the resistive SEI that continuously reforms on silicon further restricts Li^+ transport at high current densities.[61,62] Mechanical stresses are also exacerbated under fast cycling, promoting the initiation of cracks and loss of electrical connectivity within the composite.[63,64]

To confirm the cyclability potential of the I–Si/Gr samples, cycling was extended by another 100 cycles and their capacity retention was evaluated. After 200 cycles, the P–Si/Gr and I–Si/Gr electrode retains 388 mAh g^{-1} and 366 mAh g^{-1}, equivalent to 72% and 73% of its initial capacity (SI Fig. S10). This level of retention demonstrates that the green delamination method preserves substantial electrochemical activity. However, the progressive fading is consistent with known degradation pathways of Si/Gr electrodes, including fracture, SEI thickening, and loss of percolation, which is the subject of ongoing research.[65,66]

3.7 Preliminary economic analysis

A preliminary economic and environmental assessment was performed to compare the water-based delamination routes investigated in this study: ice-stripping, ultrasound delamination, and multiwashing, the latter serving as a literature-based reference process.[22,67] The system boundaries (Fig. 7a) are defined as gate-to-gate, encompassing the delamination, filtration, and drying steps required to recover battery-grade active anode material from production scrap. Downstream process stages (coating, mixing, and cell assembly) are excluded, as they are assumed to be identical for all routes and thus do not affect the comparative outcome. The analysis focuses exclusively on direct production aspects (material, energy, and water consumption), as well as the associated global warming potential (GWP), providing an initial estimate of the relative environmental and economic performance of the three delamination processes. All calculations were performed on a laboratory scale for a functional unit of 1 kg of recovered active material, as detailed in the SI (sections S1–S4). The detailed calculations are provided in the spreadsheet available in the Supplementary Information section.

Fig. 7b compares the environmental performance of the three delamination routes in terms of GWP, energy demand, and water consumption. Among the investigated methods, ice-stripping exhibits the lowest overall resource use, up to 70% lower than ultrasound delamination and multiwashing, mainly due to its short delamination time and minimal water requirement. Energy consumption is comparable for the ultrasound and multiwashing processes, while the latter requires substantially higher water input. In terms of GWP, ice-stripping achieves approximately 50% lower emissions compared to the other delamination routes and up to a 30-fold reduction relative to electrode production from pristine Si/Gr materials.

From an economic perspective, electrode manufacturing using pristine materials results in the highest costs and environmental burdens, underscoring the dual sustainability and cost advantages of implementing direct recycling approaches into manufacturing processes to utilize discarded materials and improve efficiency (Table 3). Among the three delamination routes, ice-stripping emerges as the most promising option,

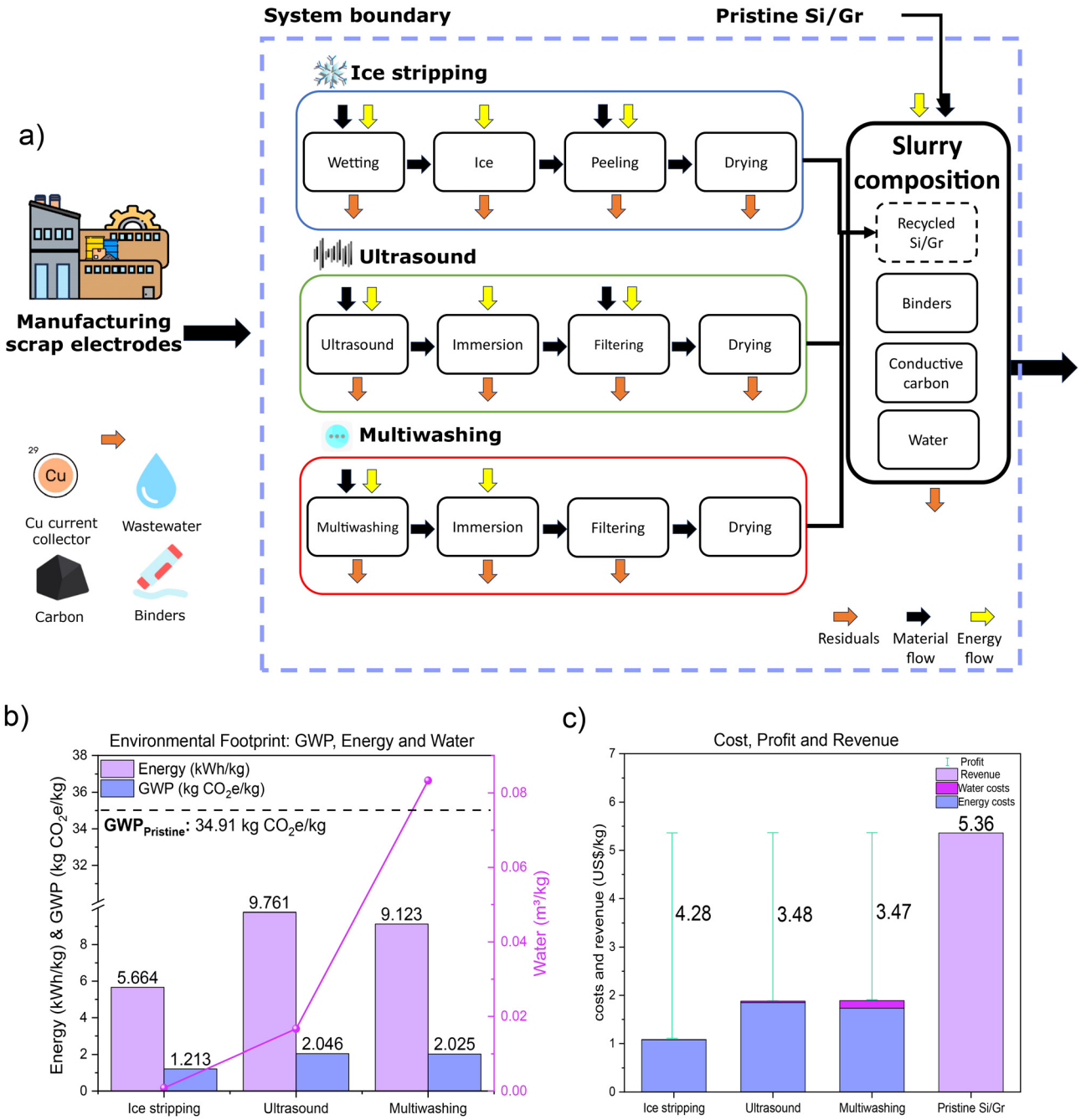

Fig. 7 (a) System boundaries for the recycling process, (b) bar chart presenting the environmental footprint, and (c) bar plot for the cost, profit, and revenue.

combining low water and energy consumption with the lowest estimated direct production costs, thereby enabling efficient remanufacturing of new electrode coatings (Fig. 7c). The analysis presented here reflects a European context; however, variations in regional cost structures and recycling practices may lead to different economic and environmental outcomes.[68]

It should be noted that this assessment is based on laboratory-scale data. Future work should therefore address the potential challenges associated with process scale-up, including higher energy requirements, optimization of the delamination process, equipment costs, and demands for wastewater treatment. While multiwashing may offer a relatively straightforward route for scale-up due to its operational simplicity, its high water use could impose significant challenges for wastewater treatment and environmental compliance. In contrast, ice-stripping demonstrates substantial potential for integration into continuous industrial processes, where its low resource demand could translate into major cost and emission savings. Incorporating these considerations into future techno-economic assessments will be crucial for validating the large-scale

Table 3 System boundary for the economic and sustainability analysis for all scenarios, showing the delamination cost, total cost (€ per kg), profit ($ per kg), and GWP (kg CO_2e per kg)

Scenario	Delam. cost (€ per kg)	Total cost (€ per kg)	Profit ($ per kg)	GWP (kg CO_2e per kg)
Ice-stripping	1.08	4.50	4.28	1.21
Ultrasound	1.88	5.30	3.48	2.05
Multiwashing	1.89	5.85	3.47	2.03
Pristine	0.00	9.13	—	34.91

The used values for the calculations are: electricity price: p_e = 0.16, € per kWh (EU non-household average, 2H2024).[69] Water price: p_w = 2.0, € per m^3 (tap water tariff, Spain). Si/Gr = 5.36, € per kg, C65 = 7.00, € per kg, CMC = 11.59, € per kg, SBR = 42.16, € per kg.[67] The emission factors were obtained from Ecoinvent 3.11 (see SI).

feasibility and sustainability of water-based delamination processes.

4. Conclusions and perspectives

To the author's knowledge, this study presents the first investigations of the direct recycling of Si/Gr composite anode scraps using environmentally benign, water-based delamination processes. We demonstrate that both ice-stripping and ultrasound delamination enable efficient separation of the active material and current collector without the use of chemical reagents or energy-intensive treatments (*i.e.*, high-temperature processes), achieving recovery efficiencies of more than 90%, while preserving key properties of the Si/Gr active material.

The structural characterizations confirm that the crystal structure of Si/Gr remains unchanged, with no evident effect on the graphitic layers or silicon phase. However, the retention of residual binder and carbon additives was detected, but with no influence on the reprocessing of the material. Minor differences were observed between the two recycled samples, mainly in the distribution of Si particles in the ultrasound-delaminated samples compared with the ice-stripped ones.

Thanks to the retention of the original binder and conductive additives, only a minor binder top-up was required during reprocessing. Electrochemical testing revealed that the ice-stripped samples exhibited the best performance among the recycled electrodes, achieving 94% of the pristine materials capacity and maintaining 74% of that capacity after 200 cycles. In contrast, the ultrasound-delaminated samples showed reduced electrochemical performance, likely due to material loss and structural damage induced by cavitation. However, further studies are needed to understand the causes of this phenomenon.

Alongside the technical validation, a preliminary cost and sustainability assessment confirms that ice-stripping is the most favorable method, offering the lowest delamination cost, lowest global warming potential (GWP), and lowest water consumption, while preserving a significant portion of the binder and conductive carbon additives. Compared with pristine electrode manufacturing, the ice-stripping route reduces total cost by approximately half and represents the most profitable of the evaluated delamination techniques.

At the current laboratory scale, both delamination methods demonstrate high recovery efficiency; however, several challenges must be addressed for industrial implementation. In the case of ice-stripping, the requirement for temperature-controlled surfaces and defrosting cycles could increase energy demand. Nonetheless, short freezing times (5–10 s) and mild operating temperatures (−5 to −10 °C) can keep specific energy consumption within reasonable limits through appropriate heat-exchange integration. While conventional ice-making equipment is unsuitable for large-scale electrode processing, an inline roll-to-roll configuration could enable continuous operation. Furthermore, depending on the geographical context, ambient environmental conditions can be leveraged to achieve the necessary freezing temperatures, thereby further improving energy efficiency.

Ultrasound delamination, by contrast, will require scaling acoustic reactors while maintaining uniform cavitation intensity. Besides high-power sonicators, which perform effectively at the laboratory scale, modular or flow-through reactor designs will be essential for continuous operation. Equipment cost and maintenance, particularly transducer lifetime, will also affect scalability. The process water can be reused in a closed-loop system following simple filtration, thereby minimizing wastewater generation. Overall, both delamination routes can benefit from energy recovery, water recirculation, and process automation, providing a viable pathway toward industrial-scale, solvent-free delamination.

Our findings confirm that ice-stripping is a practical, environmentally friendly, and cost-effective method for delaminating Si/Gr electrode scrap. Future work should focus on quantifying Si particle redistribution, optimizing binder top-up requirements after recycling, and validating process scalability through pilot-scale trials supported by full life-cycle analysis. The next logical step will be to extend this approach to cycled materials, requiring a detailed understanding of aging mechanisms and structural evolution in the complex Si/Gr composite system. Overall, this work aligns closely with the objectives of the circular economy and the emerging regulatory mandates for sustainable battery manufacturing.

Conflicts of interest

The authors have no conflicts of interest to declare.

Data availability

The data supporting this article have been included as part of the supplementary information (SI). Supplementary information is available. See DOI: https://doi.org/10.1039/d5gc04489h.

Acknowledgements

The authors are grateful to the European Commission for the support of the work, performed within the EU Horizon 2020 project HighSpin (Grant Agreement 101069508). Furthermore, the authors thank the SAFT and Talga for providing the Si/Gr material and electrode coatings.

References

1 B. Soergel, *et al.*, A sustainable development pathway for climate action within the UN 2030 Agenda, *Nat. Clim. Change*, 2021, **11**, 656–664.
2 M. S. Whittingham, Lithium Batteries: 50 years of advances to address the next 20 years of climate issues, *Nano Lett.*, 2020, **20**, 8435–8437.
3 J. R. Dahn, T. Zheng, Y. Liu and J. S. Xue, Mechanisms for lithium insertion in carbonaceous materials, *Science*, 1995, **270**, 590–593.
4 M. Je, D.-Y. Han, J. Ryu and S. Park, Constructing pure SI anodes for advanced lithium batteries, *Acc. Chem. Res.*, 2023, **56**, 2213–2224.
5 E. Feyzi, M. R. Anil Kumar, X. Li, S. Deng, J. Nanda and K. Zaghib, A comprehensive review of silicon anodes for high-energy lithium-ion batteries: Challenges, latest developments, and perspectives, *Next Energy*, 2024, **5**, 100176.
6 H. Zhou, A. Karmakar, A. S. Alujjage, B. S. Vishnugopi, J. S. Lowe, H. He and P. P. Mukherjee, Mechanistic understanding of silicon-graphite composite anode thermal stability in lithium-ion batteries, *Energy Storage Mater.*, 2025, **79**, 104334.
7 M. N. Naseer, J. Serrano-Sevillano, M. Fehse, I. Bobrikov and D. Saurel, Silicon anodes in lithium-ion batteries: A deep dive into research trends and global collaborations, *J. Energy Storage*, 2025, **111**, 115334.
8 X. Yu, W. Li, V. Gupta, H. Gao, D. Tran, S. Sarwar and Z. Chen, Current challenges in Efficient Lithium-Ion batteries' recycling: A perspective, *Global Challenges*, 2022, **6**, 2200099.
9 L. Gaines, Q. Dai, J. T. Vaughey and S. Gillard, Direct Recycling R&D at the ReCell Center, *Recycling*, 2021, **6**, 31.
10 M.-M. Titirici, *et al.*, 2024 roadmap for sustainable batteries, *J. Phys.: Energy*, 2024, 12–20.
11 A. L. Lipson, J. D. Macholz, Q. Dai, P. Melin, S. M. Gallagher, M. LeResche, B. J. Polzin and J. S. Spangenberger, Cost-Effective and Scalable Approach for the Separation and Direct Cathode Recovery from End-of-Life Li-Ion Batteries, *Adv. Energy Mater.*, 2025, 202405430.
12 M. L. Machala, X. Chen, S. P. Bunke, G. Forbes, A. Yegizbay, J. A. de Chalendar, I. L. Azevedo, S. Benson and W. A. Tarpeh, Life cycle comparison of industrial-scale lithium-ion battery recycling and mining supply chains, *Nat. Commun.*, 2025, **16**, 988.
13 E. H. Driscoll, E. Kallitsis, J. F. Marco, D. Burnett, S. Pham, R. Sommerville, L. Cooper, J. S. Edge, F. Berry, P. R. Slater, *et al.*, Grave to Cradle: A Direct Recycling Approach for Over-Discharged LiFePO4 Electric Vehicle Cells, *Adv. Energy Sustainability Res.*, 2025, 2500174.
14 M. M. Gnutzmann, A. Makvandi, B. Ying, J. Buchmann, M. J. Lüther, A. Gomez-Martin, K. Kleiner, P. Nagel, M. Winter and J. Kasnatscheew, Direct Recycling at the Material Level: Unravelling Challenges and Opportunities through a Case Study on Spent Ni-Rich Layered Oxide-Based Cathodes, *Adv. Energy Mater.*, 2024, **14**, 2400840.
15 E. C. Giles, A. Jarvis, A. T. Sargent, P. A. Anderson, P. K. Allan and P. R. Slater, Direct recycling of EV production scrap NMC532 cathode materials, *RSC Sustainability*, 2024, **2**, 3014–3021.
16 H. Ji, J. Wang, X. Qiu, H. Ren, H. Xue, H. Zhang, G. Ji, H.-M. Cheng and G. Zhou, A universal protocol for ultrafast direct regeneration and upcycling of spent lithium-ion battery cathode materials, *Nat. Protoc.*, 2025, 1–35.
17 S. L. Guzmán, M. Fehse, E. Gucciardi, M. Cabello, S. Martin, N. Etxebarria, M. Ceja, M. Romera, M. Galceran and M. Reynaud, Exploring separation techniques for the direct recycling of high voltage spinel LNMO scrap electrodes, *J. Mater. Chem. A*, 2024, **13**, 2690–2706.
18 Z. Yao, X. Ma, R. Wang, J. Hou, J. Fu, Z. Meng, P. Thanwisai, Z. Yang and Y. Wang, Recycled graphite enabled superior performance for lithium ion batteries, *J. Power Sources*, 2024, **625**, 235738.
19 B. Liu, T. Song, L. Chen, A. T. Shekhar, M. Mirolo, V. Vinci, J. Drnec, J. Cornelio, D. Xie, E. H. Driscoll, *et al.*, Sustainable Recovery and Reuse of Hard Carbon From Scrap and End-of-Life Sodium-Ion Batteries, *Adv. Energy Mater.*, 2025, 2405894.
20 A. T. Sargent, Z. Henderson, A. S. Walton, B. F. Spencer, L. Sweeney, W. R. Flavell, P. A. Anderson, E. Kendrick, P. R. Slater and P. K. Allan, Reclamation and reuse of graphite from electric vehicle lithium-ion battery anodes via water delamination, *J. Mater. Chem. A*, 2023, **11**, 9579–9596.
21 F. A. Kayakool, B. Gangaja, S. Nair and D. Santhanagopalan, Li-based all-carbon dual-ion batteries using graphite recycled from spent Li-ion batteries, *Sustainable Mater. Technol.*, 2021, **28**, e00262.
22 H. Wang, Y. Huang, C. Huang, X. Wang, K. Wang, H. Chen, S. Liu, Y. Wu, K. Xu and W. Li, Reclaiming graphite from spent lithium ion batteries ecologically and economically, *Electrochim. Acta*, 2019, **313**, 423–431.
23 J. J. Roy, D. M. Phuong, V. Verma, R. Chaudhary, M. Carboni, D. Meyer, B. Cao and M. Srinivasan, Direct recycling of Li-ion batteries from cell to pack level: Challenges and prospects on technology, scalability, sustainability, and economics, *Carbon Energy*, 2024, **6**, 1–39.
24 V. Gupta, M. Appleberry, W. Li and Z. Chen, Direct recycling industrialization of Li-ion batteries: The pre-processing barricade, *Next Energy*, 2023, **2**, 100091.
25 N. Hayagan, I. Gaalich, P. Loubet, L. Croguennec, C. Aymonier, G. Philippot and J. Olchowka, Challenges and perspectives for direct recycling of electrode scraps and

End-of-Life lithium-ion batteries, *Batteries Supercaps*, 2024, **7**, year.
26 L. Gaines, J. Zhang, X. He, J. Bouchard and H. E. Melin, Tracking flows of End-of-Life battery materials and manufacturing scrap, *Batteries*, 2023, **9**, 360.
27 IEA, *The role of critical minerals in clean energy transitions*, 2021.
28 B. Niu, J. Xiao and Z. Xu, Advances and challenges in anode graphite recycling from spent lithium-ion batteries, *J. Hazard. Mater.*, 2022, **439**, 129678.
29 L. Zhao, L. Tian, J. Li, F. Shi, Y. Chang, J. Yan and H. Zhang, Recent progress in the recycling of spent graphite anodes: Failure mechanisms, repair techniques, and prospects, *Energy Storage Mater.*, 2024, **71**, 103640.
30 Q. He, C. Guo, K. Han, F. Liu, Y. Feng, X. Wang, X. Qian and J. Meng, Direct recycling of spent graphite anode via calcium silicate coating for High-Capacity and fast lithium storage, *Carbon*, 2025, 120727.
31 L. De Vita, D. Callegari, A. Bianchi, C. Tealdi, N. Zucca, P. Galinetto, M. Colledani and E. Quartarone, A green process for effective direct recycling and reuse of graphite from End-of-Life Li-ion batteries black mass, *ChemSusChem*, 2025, 1–11.
32 D. Ruan, L. Wu, F. Wang, K. Du, Z. Zhang, K. Zou, X. Wu and G. Hu, A low-cost silicon-graphite anode made from recycled graphite of spent lithium-ion batteries, *J. Electroanal. Chem.*, 2021, **884**, 115073.
33 L. Jegan, D. S. Baji, S. Nair and D. Santhanagopalan, Sustainable mechanochemical processed recycled spent graphite and Nano-Silicon composites as anode for advanced Li-Ion batteries, *Adv. Sustainable Syst.*, 2024, **8**, 2400316.
34 E. Union, Regulation (EU) 2023/1542 of the European Parliament and of the Council of 12 July 2023 concerning Batteries and Waste Batteries, Amending Directive 2008/98/EC and Regulation (EU) 2019/1020 and Repealing Directive 2006/66/EC (Text with EEA relevance), 2023, https://eur-lex.europa.eu/eli/reg/2023/1542/oj.
35 L. Chen, B. Kishore, B. Liu, T. Song, Y. Lakhdar, O. Omoregbe, M. M. Britton, P. R. Slater and E. Kendrick, A "Cool" Route to Battery Electrode Material Recovery, *Adv. Energy Mater.*, 2025, 2405924.
36 C. Lei, I. Aldous, J. M. Hartley, D. L. Thompson, S. Scott, R. Hanson, P. A. Anderson, E. Kendrick, R. Sommerville, K. S. Ryder and A. P. Abbott, Lithium ion battery recycling using high-intensity ultrasonication, *Green Chem.*, 2021, **23**, 4710–4715.
37 C. Lei, K. S. Ryder, A. P. Abbott and J. M. Yang, Using ultrasonic Oil-Water Nano-Emulsions to purify Lithium-Ion battery black mass, *RSC Sustainability*, 2025, **3**, 1516–1523.
38 J. Rodriguez-Carvajal, Recent advances in magnetic structure determination neutron powder diffraction, *Phys. B: Condens. Matter*, 1993, **192**, 113.
39 Y. Bai, M. Li, C. J. Jafta, Q. Dai, R. Essehli, B. J. Polzin and I. Belharouak, Direct recycling and remanufacturing of anode scraps, *Sustainable Mater. Technol.*, 2022, **35**, e00542.
40 A. E. Malki, M. Asch, O. Arcelus, A. Shodiev, J. Yu and A. A. Franco, Machine learning for optimal electrode wettability in lithium ion batteries, *J. Power Sources Adv.*, 2023, **20**, 100114.
41 K. O'Regan, F. B. Planella, W. D. Widanage and E. Kendrick, Thermal-electrochemical parameters of a high energy lithium-ion cylindrical battery, *Electrochim. Acta*, 2022, **425**, 140700.
42 D. H. Jeon, Wettability in electrodes and its impact on the performance of lithium-ion batteries, *Energy Storage Mater.*, 2019, **18**, 139–147.
43 P. Zhu, E. H. Driscoll, B. Dong, R. Sommerville, A. Zorin, P. R. Slater and E. Kendrick, Direct reuse of aluminium and copper current collectors from spent lithium-ion batteries, *Green Chem.*, 2022, **25**, 3503–3514.
44 X. Bin and J. Thakur, Circular economy metrics for batteries: Enhancing sustainability in energy storage systems, *Sustain. Prod. Consumption*, 2025, **55**, 470–485.
45 I. Nuriskasari, A. Z. Syahrial, T. A. Ivandini, A. Sumboja, B. Priyono, Q. Yan, F. Destyorini and S. Priyono, Synthesis of Graphitic Carbon from Empty Palm Oil Fruit Bunches through Single-Step Graphitization Process Using K2FeO4-KOH Catalyst as Lithium Ion Battery Anode, *Results Eng.*, 2024, 103273.
46 Y. Zhang, Z. Wang, K. Hu, J. Ren, N. Yu, X. Liu, G. Wu and N. Liu, Anchoring silicon on the basal plane of graphite via a three-phase heterostructure for highly reversible lithium storage, *Energy Storage Mater.*, 2020, **34**, 311–319.
47 H. M. Albetran, Investigation of the morphological, structural, and vibrational behaviour of graphite nanoplatelets, *J. Nanomater.*, 2021, 1–8.
48 H.-J. Liang, B.-H. Hou, W.-H. Li, Q.-L. Ning, X. Yang, Z.-Y. Gu, X.-J. Nie, G. Wang and X.-L. Wu, Staging Na/K-ion de-/intercalation of graphite retrieved from spent Li-ion batteries: in operando X-ray diffraction studies and an advanced anode material for Na/K-ion batteries, *Energy Environ. Sci.*, 2019, **12**, 3575–3584.
49 O. Fromm, A. Heckmann, U. C. Rodehorst, J. Frerichs, D. Becker, M. Winter and T. Placke, Carbons from biomass precursors as anode materials for lithium ion batteries: New insights into carbonization and graphitization behavior and into their correlation to electrochemical performance, *Carbon*, 2017, **128**, 147–163.
50 J. M. Wrogemann, O. Fromm, F. Deckwirth, K. Beltrop, A. Heckmann, M. Winter and T. Placke, Impact of degree of graphitization, surface properties and particle size distribution on electrochemical performance of carbon anodes for Potassium-Ion batteries, *Batteries Supercaps*, 2022, **5**, year.
51 C. Xiao, P. He, J. Ren, M. Yue, Y. Huang and X. He, Walnut-structure Si–G/C materials with high coulombic efficiency for long-life lithium ion batteries, *RSC Adv.*, 2018, **8**, 27580–27586.
52 S. Scott, W. Du, R. Horwood, C. Lei, P. Shearing and A. P. Abbott, An assessment of blended short loop recycled graphite electrodes using X-Ray Micro-Computed tomography, *Adv. Energy Mater.*, 2025, **15**, 2403498.

53 M. Ndour, J.-P. Bonnet, S. Cavalaglio, T. Lombard, M. Courty, L. Aymard, C. Przybylski and V. Bonnet, The formulation of a CMC binder/silicon composite anode for Li-ion batteries: from molecular effects of ball milling on polymer chains to consequences on electrochemical performances, *Mater. Adv.*, 2022, **3**, 8522–8533.
54 J. Park, J. Sharma, K. W. Monaghan, H. M. Meyer, D. A. Cullen, A. M. Rossy, J. K. Keum, D. L. Wood and G. Polizos, Styrene-Based Elastomer Composites with Functionalized Graphene Oxide and Silica Nanofiber Fillers: Mechanical and Thermal Conductivity Properties, *Nanomaterials*, 2020, **10**, 1682.
55 S. Babanejad, H. Ahmed, C. Andersson, C. Samuelsson, A. Lennartsson, B. Hall and L. Arnerlöf, High-Temperature behavior of spent Li-Ion battery black mass in inert atmosphere, *J. Sustain. Metall.*, 2022, **8**, 566–581.
56 W. J. Chang, G. H. Lee, Y. J. Cheon, J. T. Kim, S. I. Lee, J. Kim, M. Kim, W. I. Park and Y. J. Lee, Direct observation of carboxymethyl cellulose and Styrene–Butadiene rubber binder distribution in practical graphite anodes for Li-Ion batteries, *ACS Appl. Mater. Interfaces*, 2019, **11**, 41330–41337.
57 S. L. Guzman, C. L. Vilumbrales, M. Reynaud, M. G. Mestres and M. Fehse, Direct recycling of cathode scrap: retain or remove residual binder and conductive carbon additives?, *J. Phys.: Energy*, 2025, **7**, 045024.
58 P. Schweigart, W. Hua, P. A. Sánchez, C. Lian, I. Nylund, D. Wragg, S. Y. Lai, F. Cova, A. M. Svensson and M. V. Blanco, Deciphering the impact of current, composition, and potential on the lithiation behavior of Si-Rich Silicon-Graphite anodes, *Small*, 2024, **21**, 2406615.
59 M. Gautam, G. K. Mishra, K. Bhawana, C. S. Kalwar, D. Dwivedi, A. Yadav and S. Mitra, Relationship between Silicon Percentage in Graphite Anode to Achieve High-Energy-Density Lithium-Ion Batteries, *ACS Appl. Mater. Interfaces*, 2024, **16**, 45809–45820.
60 Z. Yang, M. Kim, L. Yu, S. E. Trask and I. Bloom, Chemical interplay of silicon and graphite in a composite electrode in SEI formation, *ACS Appl. Mater. Interfaces*, 2021, **13**, 56073–56084.
61 E. Feyzi, X. Li, S. Deng, J. Nanda and K. Zaghib, A comprehensive review of silicon anodes for high-energy lithium-ion batteries: Challenges, latest developments, and perspectives, *Energy Next*, 2024, **5**, 100176.
62 H. Yang, S. Huang, X. Huang, W. Zhang, X. H. Liu, T. Zhu and J. Y. Huang, Kinetics-stress coupling in lithiation of Si and Ge, *Extreme Mech. Lett.*, 2015, **2**, 1–6.
63 F. Shi, P. N. Ross, G. A. Somorjai, G. Ceder, M. Z. Bazant and Y. Cui, Failure mechanisms of single-crystal silicon electrodes in lithium-ion batteries, *Nat. Commun.*, 2016, **7**, 11886.
64 V. A. Sethuraman, M. J. Chon, M. Shimshak, N. Van Winkle and P. R. Guduru, In situ measurements of stress evolution in silicon thin films during electrochemical lithiation and delithiation, *J. Power Sources*, 2011, **195**, 5062–5066.
65 H. Zhou, Q. Ma, R. Wang and Y. Zhang, Mechanistic understanding of silicon–graphite composite anode thermo-electrochemical stability in lithium-ion batteries, *Energy Storage Mater.*, 2025, **79**, 104334.
66 C. Foss, *et al.*, Revisiting Mechanism of Silicon Degradation in Li-Ion Batteries: Effect of Delithiation Examined by Microscopy Combined with ReaxFF, *J. Phys. Chem. Lett.*, 2025, **16**, 820–828.
67 M. Lechner, A. Kollenda, K. Bendzuck, J. K. Burmeister, K. Mahin, J. Keilhofer, L. Kemmer, M. J. Blaschke, G. Friedl, R. Daub and A. Kwade, Cost modeling for the GWh-scale production of modern lithium-ion battery cells, *Commun. Eng.*, 2024, **3**, year.
68 L. Schlott, M. Gutsch and J. Leker, Cost modelling and key drivers in lithium-ion battery recycling, *Nat. Rev. Clean Technol.*, 2025, 1–15.
69 Eurostat, Electricity price statistics – non-household consumers (2H2024), https://ec.europa.eu/eurostat/statistics-explained/index.php?title=Electricity_price_statistics, 2024, Accessed January 2025.